터널과 지하공간, 한국암반공학회
Vol. 11, No. 3, 2001, pp. 257~269

TUNNEL & UNDERGROUND Vol. 11, No. 3, 2001, pp. 257-269
J. of Korean Society for Rock Mech.

화강암반내 단층지역에 위치한 지하 방사성폐기물 처분장 구조거동연구

김진웅[1] · 강철형[2] · 배대석[1]

A Study on the Structural Behavior of an Underground Radwaste Repository within a Granitic Rock Mass with a Fault Passing through the Cavern Roof

Jhinwung Kim, Chulhyung Kang and Daeseok Bae

Abstract. Numerical simulation is performed to understand the structural behavior of an underground radwaste repository, assumed to be located at the depth of 500 m, in a granitic rock mass, in which a fault intersects the roof of the repository cavern. Two dimensional universal distinct element code, UDEC is used in the analysis. The numerical model includes a granitic rock mass, a canister with PWR spent fuels surrounded by the compacted bentonite inside the deposition hole, and the mixed bentonite backfilled in the rest of the space within the repository cavern. The structural behavior of three different cases, each case with a fault of an angle of 33°, 45°, and 58° passing through the cavern roof-wall intersection, has been compared. And then for the case with the 45° fault, the hydro-mechanical, thermo-mechanical, and thermo-hydro-mechanical interaction behavior have been studied. The effect of the time-dependent decaying heat, from the radioactive materials in PWR spent fuels, on the repository and its surroundings has been studied. The groundwater table is assumed to be located 10m below the ground surface, and a steady state flow algorithm is used.

Keywords: radwaste repository, granite, fault, UDEC, canister, spent fuel, bentonite, deposition hole, thermo-hydro-mechanical interaction, decay heat, steady state flow

초 록. 지하 500 m의 화강암반내 단층지역에 위치한 지하 방사성폐기물 처분장의 구조거동을 이해하기 위하여 수치해석을 수행하였다. 해석에는 2차원 해석코드인 UDEC을 사용하였다. 해석모델은 화강암반, 처분공내의 압축 벤토나이트로 둘러싸인 PWR 사용후 핵연료 처분용기 및 처분동굴내에 채워진 혼합 벤토나이트를 포함한다. 한 개의 단층이 처분동굴의 지붕과 벽이 만나는 지점을 33, 45, 및 58°의 각도로 관통하는 세가지 다른 경우에 대한 구조거동을 비교, 분석하였다. 그리고 45° 단층의 경우에 대해서는 수리역학적, 열역학적, 및 열수리역학적 상호작용 거동을 해석하고 비교, 분석하였다. PWR 사용후 핵연료내의 방사성 물질로부터 나오는 시간의존 방사성 붕괴열에 의한 영향을 해석하였다. 지하수위는 지표면 아래 10 m로 가정하였고, 지하수해석은 정류 알고리즘을 사용하였다.

핵심어: 방사성폐기물 처분장, 화강암, 단층, UDEC, 처분용기, 사용후 핵연료, 벤토나이트, 처분공, 열수리역학적 상호작용, 붕괴열, 정류

1. Introduction

High level radioactive wastes are disposed of at locations very deep underground to isolate the radioactive materials from man and his environment. The principle of the deep geological disposal is to isolate wastes from the biosphere by multiple barriers. A rock mass is the most important barrier, with granite especially being the most common and important repository host rock.

An important part of the safety evaluation of the disposal system is the assessment of the coupling effects of rock mass stability, groundwater flow, external stresses, and thermal effects. Mechanical processes affect the groundwater flow in the rock mass by changing the joint aperture. The thermal processes will result in rock expansion, which will change the joint surface and joint aperture, and could also cause convective flow of the groundwater in the joint.

Underground openings represent a region of stress

[1]한국원자력연구소
[2]정회원,한국원자력연구소
접수일 : 2001년 7월 27일
심사 완료일 : 2001년 8월 29일

release causing mechanical deformations and of pressure drop inducing groundwater flow. For hard crystalline rocks and in the presence of pre-existing joints, mechanical effects are concentrated on the joints. Redistribution of the local stress field around the opening may result in instability and release of rock blocks from walls into the opening. As excavation proceeds to form the opening, the rock responds mechanically and the joint is either opened, or compressed to a smaller aperture value. Since the mechanical compression rate is higher than the water drainage rate, water pressure builds up. This then decays after the completion of the opening and mechanical compression stabilized, and then the groundwater is allowed to drain from the joint. Rock masses are not particularly good at sustaining repeated loading and the fatigue might enhance groundwater flow and reduce their stability.

The present study is to understand the long term structural behavior of a 500 m deep hypothetical underground radwaste repository in a granitic rock mass, in which a fault with an angle intersects the roof of the repository cavern. To simplify the analysis, the symmetry in the repository layout of multiple caverns in parallel has been utilized in modeling. The data used are from references.[1,3-9]

2. Numerical model

2.1 High-level radioactive waste repository

The repository is assumed to be located at a depth of 500 m underground in a granitic rock mass with discontinuities. The caverns for the repository are 250 m long, 40 m spaced, 6m wide, and have a vertical wall height of 4.5 m and an arch shaped roof with the crown at 7 m above the cavern floor. The vertical deposition holes are located beneath the cavern floor along the centerline of the cavern at the pitch of 6m. PWR spent fuels contained in a cylindrical canister are vertically emplaced in each deposition hole. Compacted bentonite buffer material fills the area between the canister and the surrounding rock mass, and backfill material, a mixture of bentonite and crushed rock, fills the inside of the cavern(Fig. 1).

Within a corrosion resistant canister, 4 assemblies of PWR spent fuels cooled for 40 years are emplaced and fixed with a cast iron insert between the fuel assemblies and the hollow cylindrical canister.

The radioactive materials in PWR spent fuels generate decay heat through the radioactive decay process. The decay heat generated will influence the surroundings, such as the canister, buffer and backfill materials, groundwater flow, the adjacent rock mass, and the biosphere. Therefore, the behavior of the repository system should be analyzed for the decay heat generated, H(T) in w/tHM:

$$H = 2201169e^{-5.205T} + 1693.22e^{-0.018T} + 124.7e^{-0.00058T} + 19.134e^{-0.000042T} + 1.429e^{-0.000001T} \quad (1)$$

where, T is the time after discharging PWR spent fuels, $0 \leq T \leq 10^6$ years

2.2 Modeling

This numerical model is for the simulation of the coupled behavior between thermal, hydraulic, and mechanical interaction using a steady state flow algorithm for the long term behavior(500 years) of a radioactive waste repository in which heat producing wastes are placed vertically beneath the cavern floor.

The top and bottom horizontal boundaries are moved sufficiently far from the heat generating waste. The excavation of the disposal cavern, waste emplacement, and buffer filling are all assumed to be instantaneous, and the initial horizontal stress is assumed to be equal to the initial vertical stress in the analysis.

Waste canisters are located at a pitch of 6 m below the cavern floor along the centerline of the disposal cavern. In order to do the two dimensional approximation using the UDEC code, this discrete waste location is distributed uniformly along the disposal cavern. This means that the heat generating trench is located below the cavern floor along the centerline of the disposal cavern.

The tributary heating area is 10,000 m^2, which is equal to the area of the cavern length of 250 m multiplied by the cavern spacing of 40 m. Heat flux is obtained by the following processes :

(1) decay heat in w/tHM is multiplied by the weight of the 4 fuel assemblies, and then divided by the area of the pitch of 6 m multiplied by the cavern spacing of 40 m, (2) the value obtained from (1) above is

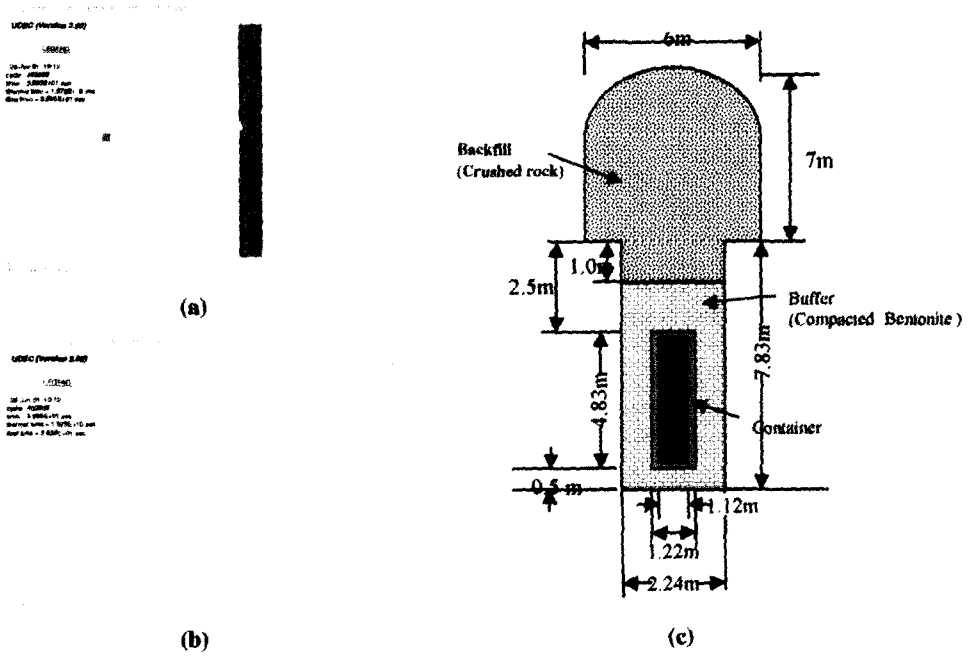

Fig. 1. The (a) numerical model and (b) enlarged view of the model, and (c) a cavern and a deposition hole with a canister.

multiplied by the tributary heating area of 10,000 m^2 and then divide by the cavern length of 250 m. Here, offset distances, 12 m and 13 m, on both ends of the cavern should be considered, (3) then, heat flux, F, is the value from (2) above divided by the area of the heat source.

$$F = (28.0554)e^{-(5.708E-10)t} + (4.1492)e^{-(1.839E-11)t} + (0.6486)e^{-(1.332E-12)t} + (0.04876)e^{-(3.171E-14)t} \quad (2)$$

where, t is the time after 40 years of cooling, $0 \leq t \leq 3.1536E13$ sec, F in w/m^2.

Granitic rock mass is assumed as homogeneous and isotropic with elastoplastic behavior(Mohr-Coulomb failure criteria applied), and compacted and mixed bentonite are regarded as elastoplastic material(Drucker-Prager failure criteria applied). The material for the canister is assumed to be homogeneous, isotropic, and linearly elastic. The Barton-Bandis joint constitutive model, a non-linear joint model that directly utilizes properties from laboratory tests on joints derived by Drs. Nick Barton and Stravros Bandis at the Norwegian Geotechnical Institute[ref. 2], is used for the rock joints.

For the hydraulic analysis using a steady state flow algorithm, groundwater flows through the discontinuities of the rock mass. A fully coupled hydro-mechanical analysis is performed in which fracture conductivity is dependent on mechanical deformation of the joint aperture; conversely, joint water pressures affect the mechanical behavior. Groundwater flow is idealized as laminar viscous flow.

For the thermal analysis, this model simulates transient heat conduction in materials and the subsequent development of thermally induced displacements and stresses. Heat transfer is modeled as isotropic conduction and heat decays exponentially with time. The thermal analysis provides only one way coupling to the mechanical stress calculation through the thermal expansion coefficient and to the calculation for groundwater flow in joints through the temperature dependency of groundwater density and joint permeability.

2.3 Initial and boundary conditions

The boundary conditions for this fully saturated 200 m model are fixed horizontal displacements on both sides, fixed vertical displacement at the bottom, and free at the surface. Impermeable boundary con-

ditions are assumed on both sides and at the bottom of the model. The thermal boundary conditions are adiabatic on both sides and at the bottom. The initial temperature is assumed to be 32°C at the top and to increase 0.6°C for every 20 m and 38°C at the bottom of the model.

2.4 Material properties

Material properties for the host granitic rock, rock fault, compacted and mixed bentonite, and canister cast iron insert are as follows[1,3-9]:

3. Results of the analysis

3.1 Three cases with different fault angles

The structural behavior of three different cases, each case with a fault of an angle of 33°, 45°, and 58° passing through the roof-wall intersection of the repository cavern, has been compared. The model used for comparison purposes is the coupled thermo-hydro-mechanical interaction model fully saturated for a period of 50 years, which approximately corresponds to the time period of reaching the maxi-mum temperature on the model due to the decaying heat from radioactive materials.

The maximum values of the displacements and principal stresses on the rock mass of the model with different fault angles are in Table 6. The displacement in the case with a 58° fault angle is the largest, but the

Table 1. Mechanical and thermal properties of granite.

Parameter	Value
density	2700.0 kg/m^3
bulk modulus	40.0 GPa
shear modulus	24.0 GPa
thermal conductivity	3.2 W/mC
thermal expansion coeff.	8.3E-6 1/°C
specific heat	815.0 J/kgC
friction angle	25.0°
cohesion	16.0 MPa
dilation	8.0

Table 2. Mechanical properties of a fault.

Parameter	Value
joint normal stiffness	1.6E4 GPa/m
joint shear stiffness	7.0E3 GPa/m
joint cohesion	0.1 MPa
joint dilation	0.0°
joint aperture	1.0E-2 m
joint permeability	3.0 1/(Pa*sec)
joint residual aperture	5.0E-4 m
joint length	0.1 m
joint roughness coeff.	5.0
joint comp. strength	30.0 MPa
residual angle of friction	45.0°
intact rock comp. str.	200.0 MPa

Table 3. Mechanical and thermal properties of compacted bentonite.

Parameter	Value
density	2100.0 kg/m^3
bulk modulus	3.5 GPa
shear modulus	0.75 GPa
thermal conductivity	1.2 W/mC
thermal expansion coeff.	0.0 1/°C
specific heat	1000.0 J/kgC

Table 4. Mechanical and thermal properties of mixed-bentonite.

Parameter	Value
density	2100.0 kg/m^3
bulk modulus	3.33 GPa
shear modulus	1.54 GPa
thermal conductivity	2.0 W/mC
thermal expansion coeff.	8.3E-6 1/°C
specific heat	800.0 J/kgC

Table 5. Mechanical and thermal properties of canister cast iron insert.

Parameter	Value
density	8000.0 kg/m^3
bulk modulus	167.0 GPa
shear modulus	77.0 GPa
thermal conductivity	15.2 W/mC
thermal expansion coeff.	8.2E-6 1/°C
specific heat	504.0 J/kgC

Table 6. Maximum results on the model with different fault angles.

Results\Fault angles	33°	45°	58°
displ. vectors (m)	5.59E-2	5.647E-2	5.841E-2
principal stresses (Pa)			
min.	-9.176E7	-9.175E7	-9.15E7
max.	2.444E6	2.533E6	3.052E6
shear displ. (m)	1.827E-3	1.941E-3	2.396E-3

differences in the other two cases are less than 5%. The maximum values of the principal stress and shear displacement on the model with a 58° fault are 3.052 MPa and 2.396 mm which are 16%~20% and 19%~24% larger than the results on the other two models, respectively. But the magnitude of the tensile stress of 3.052 MPa is not very significant, and the maximum shear displacement of 2.396 mm at the middle of the line of the fault is due to the high fault angle. In all three cases, the locations of the maximum value of the principal stress, displacement vector, and shear displacement are the rock just below the deposition hole, the top of the model, and the middle of the line of the fault, in that order. The displacements and principal stresses in the vicinity of the cavern are summarized in Table 7.

The displacements, in general, are larger in the case with a 58° fault angle than in the other two cases. The maximum principal stress near the cavern roof-wall intersection is -14.65 MPa on the model with a 33° fault which is 34%~46% larger than the results on the other two models, but the magnitude of the compressive stress is not very significant. The minimum principal stress at the location underneath the deposition hole are larger in the case with a 33° fault angle. But the differences in all three cases are very small.

3.2 Coupling behavior between thermal, hydraulic, and mechanical interactions

Three different cases of coupling behavior between thermal, hydraulic, and mechanical interactions have been studied and compared. The model used here for comparison purposes is the 200 m model with a 45° fault intersecting the cavern roof-wall intersection.

The first case is the hydro-mechanical(HM) model using a steady state flow algorithm. The second case is the thermo-mechanical(TM) model in a dry condition without groundwater for a period of 50 years after the emplacement of the canister and filling with buffer materials. The last case is the thermo-hydro-mechanical(THM) model fully saturated using a steady state flow algorithm for a period of 50 years after the emplacement of the canister and filling with buffer materials.

The maximum values of the structural responses on the model for three different cases are summarized below in Table 8~10. The maximum values of the displacement vector, shear displacement, principal stresses, and hydraulic aperture on the rock mass of the model are in Table 8.

The THM model shows the largest values of the hydraulic aperture, displacement vector, shear displacement, and minimum principal stress. The minimum principal stress on the THM model is -91.68 MPa which is 2.4% larger than that on the TM model. The shear displacement and hydraulic aperture on the THM model are 1.932 mm and 0.4816 mm which are approximately 7%~12.5% larger than those on the TM model, respectively. The locations of the maximum value of the principal stress, displacement vector, shear displacement, and hydraulic aperture are the rock just below the deposition hole, the top of the model, the middle of the fault line, and the fault end away from the cavern in the TM and THM models, and the rock above the top of the cavern wall, the deposition hole-cavern floor intersection, the rock close to the canister center, and the rock along the horizontal line connecting the canister center in the HM model, in that order. The HM model shows the smallest values among all the results.

Table 7. Results in the vicinity of the repository cavern with different fault angles.

Results\Fault angles	33°	45°	58°
displ. vectors (m)			
@cavern crown	3.374E-2	3.419E-2	3.549E-2
@dep. hole-cavern floor intersection	2.981E-2	3.004E-2	3.083E-2
@roof-wall intersection	3.175E-2	3.203E-2	3.309E-2
principal stresses (Pa)			
near roof-wall intersection			
min.	-6.702E7	-6.606E7	-6.394E7
max.	-1.465E7	-9.703E6	-7.978E6
underneath the dep. hole			
min.	-9.176E7	-9.175E7	-9.150E7
max.	-2.552E7	-2.554E7	-2.455E7

Table 8. Maximum values on the rock mass of the model.

Results\Cases	HM Model	TM Model	THM Model
displ. vectors (m)	1.625E-3	5.633E-2	5.649E-2
principal stresses (Pa)			
min.	-2.581E7	-8.946E7	-9.168E7
max.	-1.932E4	4.097E6	2.554E6
shear displ. (m)	1.042E-3	1.69E-3	1.932E-3
hydraulic aperture (m)	4.311E-4	4.468E-4	4.816E-4

Table 9. Maximum values on the fault of the model.

Results\Cases	HM Model	TM Model	THM Model
normal stresses (Pa)			
min.	4.393E6	1.081E-1	2.694E-10
max.	1.579E7	3.452E7	2.952E7
shear stresses (Pa)			
min.	-2.268E5	-8.713E6	-7.926E6
max.	6.113E5	1.081E-1	9.268E-11
normal displ. (m)			
min.	-4.292E-9	-6.797E-9	-1.833E-9
max.	1.837E-9	2.274E-4	2.623E-4
shear displ. (m)			
min.	-1.72E-4	1.837E-4	2.747E-4
max.	1.182E-4	1.69E-3	1.932E-3
hydraulic aperture (m)			
min.	2.194E-4	2.194E-4	2.194E-4
max.	2.194E-4	4.468E-4	4.816E-4

Table 10. Maximum values in the vicinity of the cavern on the model.

Results\Cases	HM Model	TM Model	THM Model
displ. vectors (m)			
@cavern crown	7.777E-4	3.429E-2	3.419E-2
@cavern roof-wall intersection	9.368E-4	3.211E-2	3.203E-2
@cavern floor-dep. hole intersection	1.625E-3	3.005E-2	3.004E-2
principal stresses (Pa) near cavern roof-wall intersection on the rock mass			
min.	-2.581E7	-6.573E7	-6.599E7
max.	-1.463E7	-1.058E7	-9.733E6
underneath the deposition hole on the rock mass			
min.	-2.455E7	-8.946E7	-9.168E7
max.	-1.611E7	-2.514E7	-2.556E7

The values of the normal and shear stresses and displacements, and hydraulic aperture on the fault of the model are shown in Table 9. The maximum normal and the minimum shear stresses are larger on the TM model than on the THM model. The normal stress of 34.52 MPa on the TM model is 14.5% larger than that on the THM model. The maximum values of the normal and shear displacements and hydraulic aperture are larger on the THM model than on the TM model. The minimum shear displacement shows approximately 33% larger value on the THM model than on the TM model. The results on the HM model are the smallest.

The maximum values of displacement vectors and principal stresses in the vicinity of the cavern on the model are summarized in Table 10. The results on the TM and THM models do not show much difference, but the results on the HM model are the smallest of all the results.

3.3 Thermo-hydro-mechanical interaction behavior

The structural behavior of the coupled thermo-hydro-mechanical interaction on a 200 m fully saturated model with a 45° fault passing through the cavern roof-wall intersection has been studied.

At the initial stage, the loads acting on the model are mainly the weight of the fully saturated granitic rock mass except for the ground temperature of 32°C on the top of the model and of 0.6°C increase for every 20 m below the top boundary.

The distributions of the vertical and horizontal stresses are shown in Fig. 2(a) and (b), respectively. The maximum and minimum vertical stresses are approximately 15 MPa near the bottom and 11 MPa near the top of the model, respectively. Horizontal stresses are approximately 16 MPa near the bottom and 11 MPa near the top of the model.

Excavation of the cavern and the deposition hole is assumed to be instantaneous. The displacement vectors right after excavation are shown in Fig. 2(c). Maximum displacement of 1.268 mm, in the direction of the excavated zone, occurs at the intersection of the deposition hole and the cavern floor. The cavern crown displaces 0.44 mm downward, and the intersection of the cavern roof and the line of the fault displaces 0.63 mm toward the excavated zone in the direction of the line of the fault. The point on the rock mass at the location of the center of the deposition hole displaces 1.2 mm toward the excavated zone.

Canister emplacement, and compacted and mixed bentonite filling are also assumed to be instantaneous. The displacement vectors are shown in Fig. 2(d). The intersection of the deposition hole and the cavern floor displaces 1.635 mm toward the center of the cavern floor. The cavern crown displaces 0.75 mm downward, the fault-roof intersection moves 0.92 mm toward the inside of the cavern, and the rock near the center of the deposition hole displaces 1.42 mm toward the deposition hole.

Results from the analysis of the THM model are shown in Figs. 3, 4, 5, 6, and 7. The temperature

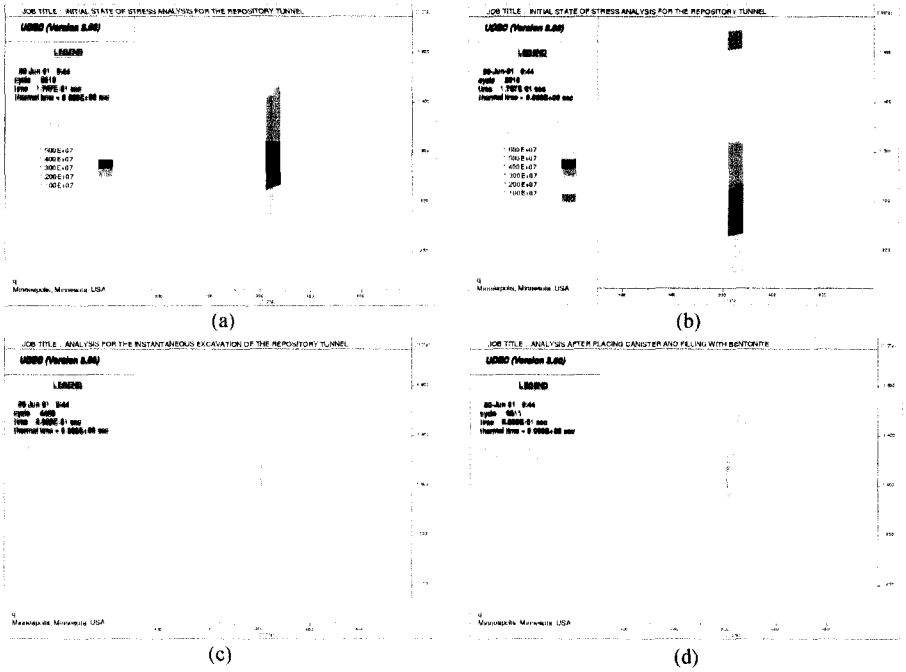

Fig. 2. The (a) vertical and (b) horizontal stress distributions at initial stage, and displacement vectors (c) right after excavation and (d) after filling with buffer materials.

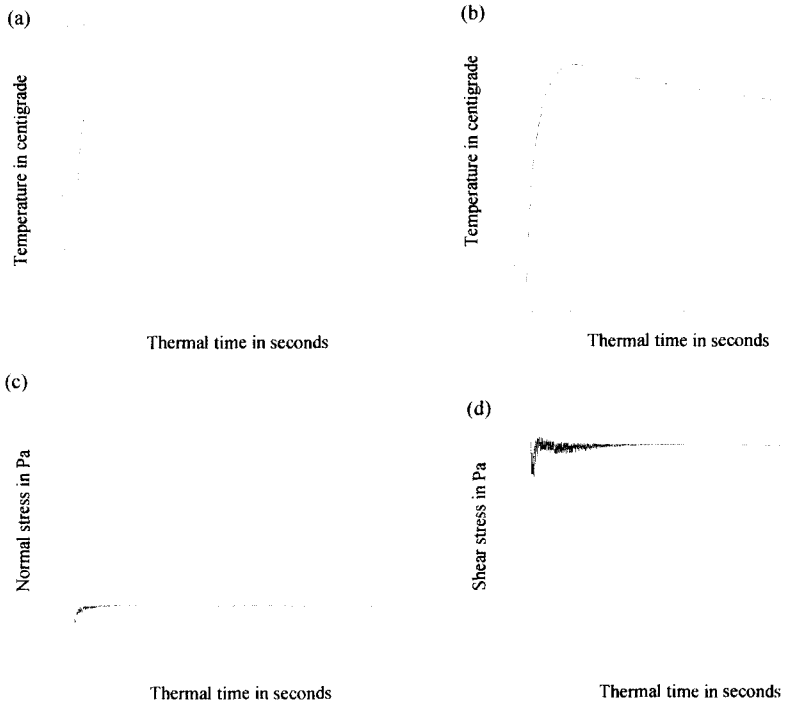

Fig. 3. Temperature histories (a) along the level of the canister center and (b) along the cavern floor level, and (c) normal and (d) shear stress histories for the period of 500 years after waste emplacement.

histories from the analysis for a period of 500 years from the waste emplacement are shown in Fig. 3(a) and (b). Fig. 3(a) shows the temperature histories of the points along the horizontal line starting from the center of the canister, the interfaces of the canister and the compacted bentonite and the rock, and points on the rock mass. The temperatures reach maximum values at the points mentioned above after 55~60 years from the waste emplacement. And then the temperature decays for the rest of the period. Fig. 3(b) shows the temperature histories of the points along the cavern floor starting from the center of the cavern floor, cavern floor-deposition hole intersection, and cavern floor rib intersection. The temperature at these points reach maximum values after 75~85 years which is 15~25 years later than the previously mentioned times.

Normal and shear stress histories for a period of 500 years after the waste emplacement are shown in Figs. 3(c) and (d) for the points on the rock close to the cavern wall. Histories for the points on the rock close to the cavern wall, on the cavern floor level, crown level, and the level of wall-roof intersection converge fastly to the values of -2.9, 30, and -1.5 MPa for the normal stress, and -3.3, 0.6, and -1 MPa for the shear stress, in that order.

Normal displacement histories for a period of 500 years after the waste emplacement are shown in Fig. 4. The histories shown are for the points at the cavern crown in Fig. 4(a), at the cavern floor center in Fig. 4(b), at the cavern floor-deposition hole intersection in Fig. 4(c), and at the cavern roof-wall intersection in Fig. 4(d). In Fig. 4(d), many oscillations on the normal displacement history are shown. This is due to the fact that the line of the fault also intersects the cavern wall-roof intersection and this zone is the most highly stressed of all the zones on the model.

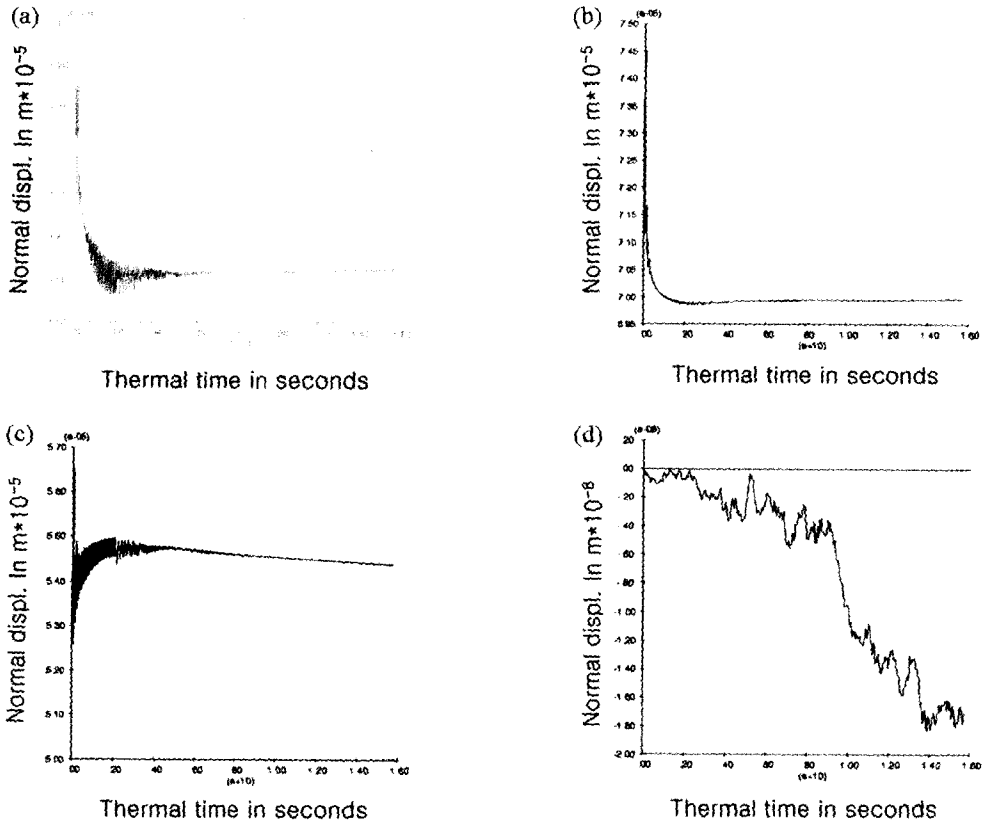

Fig. 4. Normal displacement histories (a) on the cavern crown, (b) on the cavern floor center, (c) on the cavern floor-deposition hole intersection, and (d) on the cavern roof-wall intersection for the period of 500 years after waste emplacement.

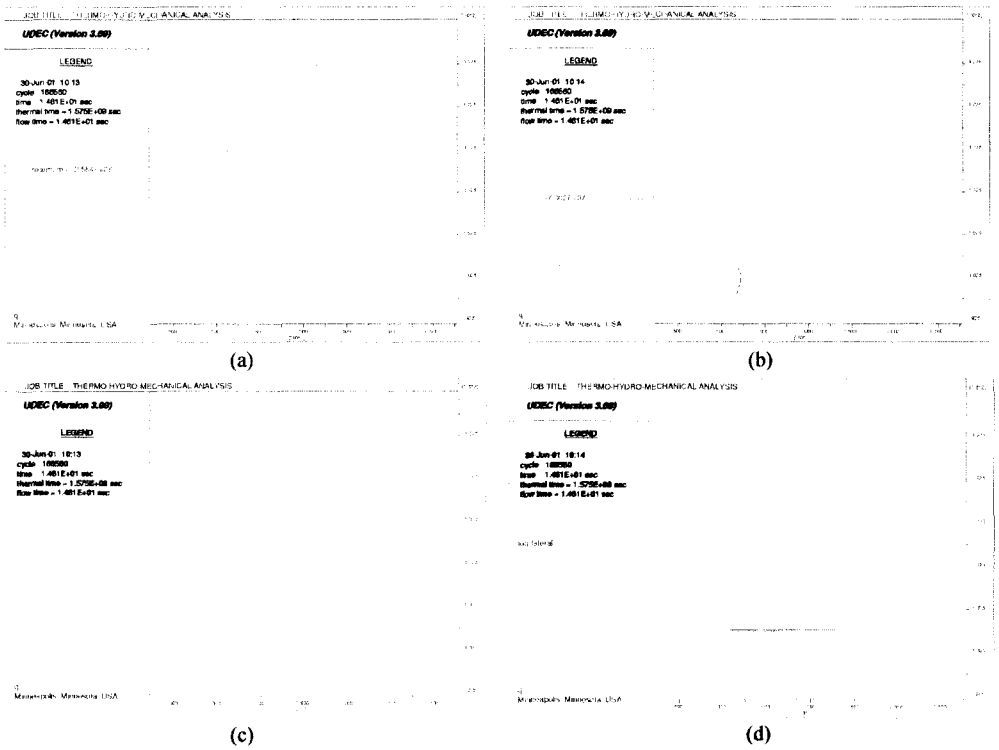

Fig. 5. The (a) principal and (b) major principal stress distributions, and (c) displacement vectors and (d) shear displacement distribution after 50 years from waste emplacement.

Results of the analysis for a period of 50 years after the waste emplacement are summarized below and shown in Figs. 5, 6, and 7. The temperature reaches maximum values approximately after 50 years from the waste emplacement, as shown in Figs. 3(a) and (b). The principal and major principal stress contours are shown in Figs. 5(a) and (b), and the range of the stresses are -91.68 MPa~2.554 MPa. The displacement vectors and the shear displacement distribution are shown in Figs. 5(c) and (d). Most of the displacements are directed upward due to the high temperature distributions.

Fig. 5(c) shows large displacements along the line of the fault and the largest upward displacement of 3.95 cm at the end of the fault line away from the cavern. The upward displacement distributions are 3.42 cm at the crown, 3.3 cm at the center of the mixed bentonite, 3.18 cm at the wall-roof intersection, 2.97 cm at the floor center, and 2.61 cm at the center of the deposition hole. Fig. 5(d) shows the shear displacement distributions, and the shear displacements are 1.93 cm at around the middle of the fault line, 1.51 mm on the rock near the center of the deposition hole, and 0.85 mm at the cavern floor-deposition hole intersection.

The temperature distribution on the model is shown in Fig. 6(a) and its enlarged view near the repository is shown in Fig. 6(b).

Normal and shear stress distributions along the 45° fault line are shown in Figs. 6(c) and (d). Normal stress distributions on the fault line are 30 MPa approximately at the cavern wall location and 0 on the other end of the fault line. Shear stress distributions show -3 MPa at the cavern wall location, -8 MPa at the location 6 m away from the wall, and 0 at the right end of the fault line.

Fig. 7 shows the variations of the hydraulic aperture, domain pressure, flow rate, and mean flow velocity along the fault line. The initial aperture of the fault is 1.0 cm. After 50 years from the waste emplacement,

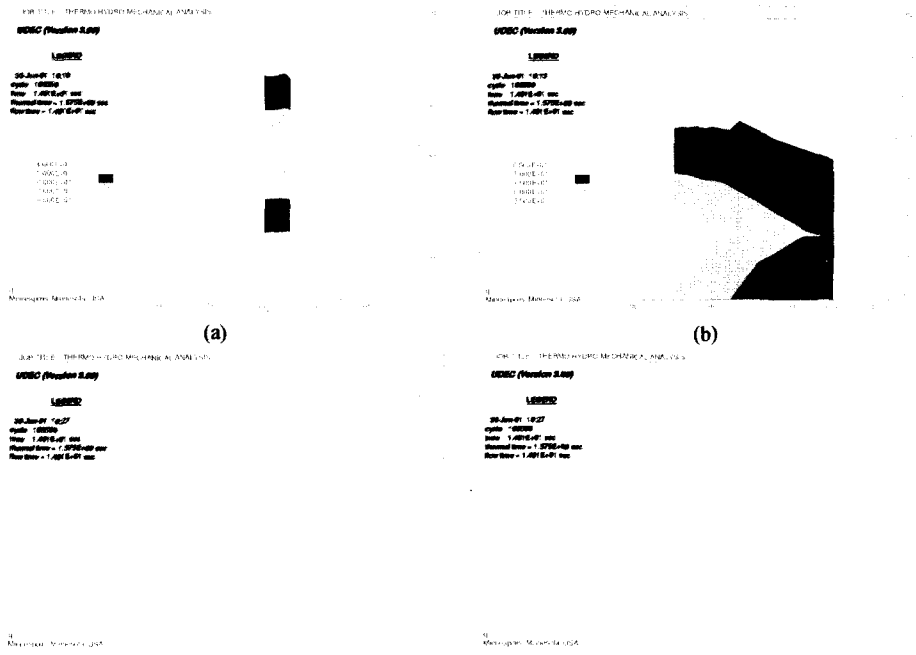

Fig. 6. The (a) temperature distribution on the model, (b) its enlarged view, (c) normal and (d) shear stress distributions along the 45 degree fault line after 50 years from waste emplacement.

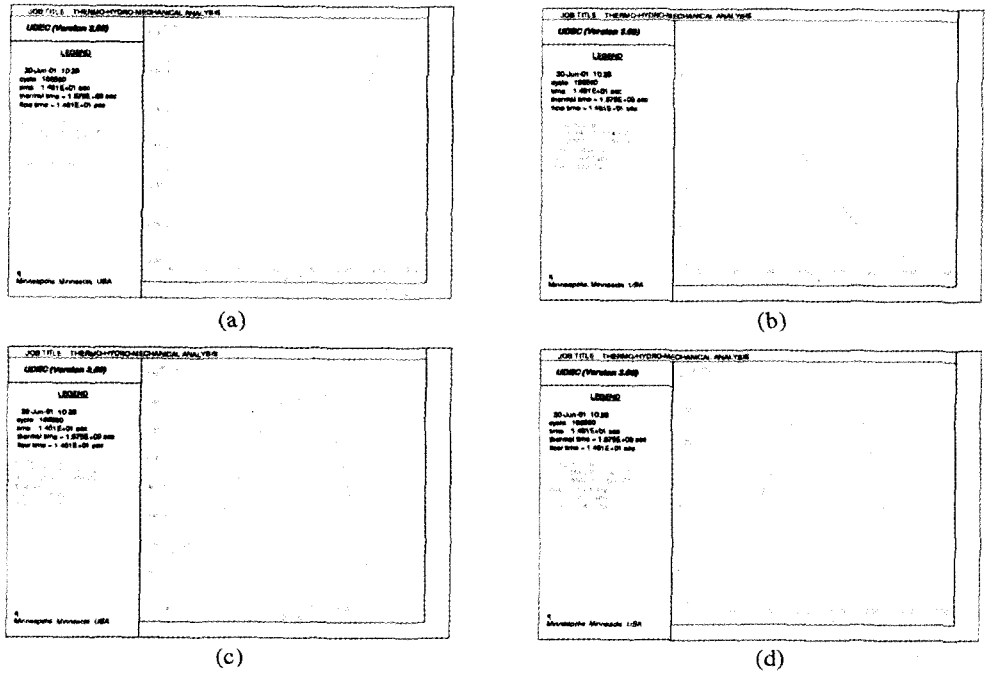

Fig. 7. Variations of (a) the hydraulic aperture, (b) domain pressure, (c) flow rate, and (d) mean flow velocity along the 45 degree fault line after 50 years from waste emplacement.

the hydraulic aperture distributions show 0.22 mm at the location of the cavern wall and constant for the length of 18 m along the fault line and then a linear increase up to 0.48 mm at the other end of the fault line as shown in Fig. 7(a). The maximum hydraulic conductivity here is 1.0E-2 cm^2. Domain pressure distributions are shown in Fig. 7(b) and the pressure of 4.63 MPa at the location of the cavern wall decreases slightly at the other end of the fault line. The flow rates in Fig. 7(c) show 0.3E-11 m^3/sec at the cavern wall location, a maximum value of 1.5E-11 m^3/sec at the location 18 m away, and then 0 at the other end of the fault line. The mean flow velocities in Fig. 7(d) show 1.4E-6 m/sec at the location of the cavern wall, 6.7E-6 m/sec at the location 18 m away, and then 0 at the other end of the fault line.

4. Conclusion

The numerical model studied here is a 500 m deep underground radwaste repository in a granitic rock mass, in which a fault passes through the cavern roof-wall intersection of the repository cavern. Within the repository cavern, a canister with heat generating PWR spent fuels is emplaced in the deposition hole, and compacted bentonite fills the area between the canister and the wall of the deposition hole. Then, mixed bentonite is backfilled in the remaining space within the repository cavern. A two dimensional code, UDEC, is used for the analysis of the model.

The structural behavior of three different cases, each case with a fault of an angle of 33, 45, and 58° passing through the cavern roof-wall intersection has been studied and compared using the coupled thermo-hydro-mechanical model fully saturated for a period of 50 years from the waste emplacement. For the three different cases the maximum values of the displacement vectors, principal stresses, and shear displacements on the model have been compared. The effect of the change of the fault angle, on the range studied here, is very much local and the effect on the overall structural stability of the model is not significant.

Three different cases of coupling behavior between thermal, hydraulic, and mechanical interactions have been studied and compared. The model used here for comparison purposes is the 200 m model with a 45° fault intersecting the cavern roof-wall intersection. The first case is the hydro-mechanical model, and the second case is the thermo-mechanical model under a dry condition for a period of 50 years, and the last case is the thermo-hydro-mechanical model fully saturated for a period of 50 years after the emplacement of the canister and filling with buffer materials. The magnitude of the results, in general, are larger on the THM model and much smaller on the HM model, and the effect of the decaying heat from the radioactive materials in PWR spent fuels is a dominating factor on the structural performance of the model.

The coupled thermo-hydro-mechanical interaction behavior on a fully saturated model with a 45° fault passing through the cavern roof-wall interaction has been studied. The maximum and minimum vertical stresses are approximately 15 MPa at the bottom and 11 MPa at the top of the model in the initial stage. Upon instantaneous excavation, the displacements are 0.44 mm at the cavern crown, 0.63 mm at the cavern roof-wall-fault intersection, and 1.2 mm at the point on the rock mass close to the center of the deposition hole. These displacements are all directed toward the excavated zone. Just after the canister emplacement and buffer filling the displacements are 1.635 mm at the point on the rock where the deposition hole intersects the cavern floor, 0.75 mm at the cavern crown, and 0.92 mm at the roof-wall-fault intersection. These displacements are all directed toward the center of the cavern.

For a period of 500 years from the waste emplacement, the temperature distributions at the locations along the horizontal line starting from the center of the canister show maximum values after approximately 55 ~60 years from the waste emplacement, and then decay for the rest of the period. Normal and shear stress, and normal displacement histories show a fast convergence. Normal displacement history at the cavern roof-wall intersection shows many oscillations. This is due to the fact that the line of the fault also passes through this intersection, and this zone is the most highly stressed of all the zones on the model.

The coupled thermo-hydro-mechanical interaction behavior has been studied for a period of 50 years from the waste emplacement which corresponds to the period of reaching the maximum temperature on the model.

The principal stress distributions on the model are in the range of -91.68 MPa~2.554 MPa. The displacements on this model are rather high and directed upward due to the high temperature distributions. The displacements are 3.95 cm upward at the end of the fault line away from the cavern, 3.42 cm upward at the crown, 3.3 cm at the center of the mixed bentonite, 3.18 cm at the wall-roof intersection, and 2.97 cm at the floor center. The shear displacements are 1.93 cm at around the middle of the fault line, and 1.51 mm on the rock near the center of the deposition hole. The initial aperture of the fault is 1.0 cm. After 50 years from the waste emplacement, the hydraulic aperture distributions show 0.22 mm at the location of the cavern wall and constant for the length of 18 m along the fault line and then a linear increase up to 0.48 mm at the other end of the fault line. The maximum hydraulic conductivity here is 1.0E-2 cm^2. The maximum flow rate and flow velocity are 1.5E-11 m^3/sec and 6.7E-6 m/sec, respectively, at the location 18 m away on the fault line.

Acknowledgement

The present study is financially supported by the National Long Term Nuclear R&D Fund from the Ministry of Science and Technology.

References

1. Kang, Chulhyung et al, 2000, Preliminary conceptual design and performance assessment of a deep geological repository for high-level waste in the Republic of Korea, KAERI and Sandia National Lab., Rep. of Korea.
2. Itasca Consulting Group, Inc., 1996, UDEC(Universal Distinct Element Code), version 3.0, Minneapolis, Minnesota, USA.
3. Hudson, J.A., ed. in chief, 1993, Comprehensive Rock Engineering: surface and underground project case histories, vol. 5, Pergamon Press, NY.
4. Hokmark, H. and I. Israelsson, 1991, Distinct element modelling of joint behavior in nearfield rock, Stripa Project 91-22, SKB, Sweden.
5. Hokmark, H., 1990, Distinct element method of fracture behavior in near field rock, Stripa Project 91-01, SKB, Sweden.
6. Johansson, E., M. Hakala, and L.J. Lorig, 1991, Rock mechanical, thermomechanical, and hydraulic behavior of the near field for spent nuclear fuel, Report YJT-91-21, TVO, Helsinki, Finland.
7. SKB, 1997, Results from pre-investigations and detailed site characterizations: Summary Report, Aspo HRL-Geoscientific Evaluation 1997/2, SKB Technical Report 97-03, Sweden.
8. Hakala, M., E. Johansson, A. Simonen, and L. Lorig, 1993, Application of the continuously yielding joint model for studying disposal of high-level nuclear waste in crystalline rock, Report YJT-93-06, TVO, Helsinki, Finland.
9. SKB, 1997, Results from pre-investigations and detailed site characterization: Summary Report, Aspo HRL-Geoscientific Evaluation 1997/2, SKB Technical Report 97-04, Sweden.

김 진 웅

1971년 Iowa State University, Civil Engineering, BS degree
1973년 University of Iowa, Structural engineering, MS degree
1983년 Cornell University, Structural Engineering, PhD degree
Tel : 042-868-2018
E-mail : njwkim@kaeri.re.kr
현재 한국원자력연구소 방사성폐기물처분연구팀 팀장

강 철 형

1977년 서울대학교 공과대학 원자핵공학과 공학사
1983년 워싱턴 대학교 대학원 원자핵공학과 공학석사
1989년 캘리포니아 대학교 대학원 원자핵공학과 공학박사
Tel : 042-868-8914
E-mail : chkang@kaeri.re.kr
현재 한국원자력연구소 책임연구원

배 대 석

1976년 경북대학교 문리과대학 지질학과, 이학사
1990년 충남대학교 대학원 지질학과 이학석사
1996년 충남대학교 대학원 지질학과 이학박사
Tel : 042-868-2030
E-mail : ndsbae@kaeri.re.kr
현재 한국원자력연구소 방사성폐기물처분연구팀, 책임연구원